Blue straggler stars in dwarf spheroidal galaxies

Mapelli, M.; Ripamonti, E.; Tolstoy, E.; Sigurdsson, S.; Irwin, M. J.; Battaglia, G.

Published in:
Monthly Notices of the Royal Astronomical Society

DOI:
10.1111/j.1365-2966.2007.12148.x

Publication date:
2007

Mon. Not. R. Astron. Soc. **380,** 1127–1140 (2007) doi:10.1111/j.1365-2966.2007.12148.x

Blue straggler stars in dwarf spheroidal galaxies

M. Mapelli,[1⋆] E. Ripamonti,[2] E. Tolstoy,[2] S. Sigurdsson,[3] M. J. Irwin[4] and G. Battaglia[2]

[1]*Institute for Theoretical Physics, University of Zürich, Winterthurerstrasse 190, CH–8057 Zürich, Switzerland*
[2]*Kapteyn Astronomical Institute, University of Groningen, Postbus 800, 9700 AV Groningen, the Netherlands*
[3]*Department of Astronomy and Astrophysics, The Pennsylvania State University, 525 Davey Lab, University Park, PA 16802, USA*
[4]*Royal Greenwich Observatory, Madingley Road, Cambridge CB3 0EZ*

Accepted 2007 June 22. Received 2007 June 22; in original form 2007 June 4

ABSTRACT

Blue straggler star (BSS) candidates have been observed in all old dwarf spheroidal galaxies (dSphs), however whether or not they are authentic BSSs or young stars has been a point of debate. To both address this issue and obtain a better understanding of the formation of BSSs in different environments, we have analysed a sample of BSS candidates in two nearby Galactic dSphs, Draco and Ursa Minor. We have determined their radial and luminosity distributions from wide field multicolour imaging data extending beyond the tidal radii of both galaxies.

BSS candidates are uniformly distributed through the host galaxy, whereas a young population is expected to show a more clumpy distribution. Furthermore, the observed radial distribution of BSSs, normalized to both red giant branch (RGB) and horizontal branch (HB) stars, is almost flat, with a slight decrease towards the centre. Such a distribution is at odds with the predictions for a young stellar population, which should be more concentrated. Instead, it is consistent with model predictions for BSS formation by mass transfer in binaries (MT-BSSs). Such results, although not decisive, suggest that these candidates are indeed BSSs and that MT-BSSs form in the same way in Draco and Ursa Minor as in globular clusters. This favours the conclusion that Draco and Ursa Minor are truly 'fossil' galaxies, where star formation ceased completely more than 8 billion years ago.

Key words: stellar dynamics – blue stragglers – galaxies: dwarf – galaxies: individual: Draco – galaxies: individual: Ursa Minor.

1 INTRODUCTION

Blue straggler stars (BSSs) are stars located above and blue-ward of the main sequence (MS) turn-off in a colour–magnitude diagram (CMD). They were first discovered in a globular cluster (M3; Sandage 1953), and are mainly observed in star clusters (Fusi Pecci et al. 1992; Ferraro et al. 1993, 1997, Zaggia, Piotto & Capaccioli 1997, Ferraro et al. 2003, 2004; Sabbi et al. 2004; Hurley et al. 2005, Lanzoni et al. 2007a,b, and references therein) where the tiny (if any) spread in the stellar age makes their identification straight forward. However, there have been attempts to find halo BSSs in the Milky Way, which show up as high-velocity stars brighter and hotter than turnoff stars in the Galactic halo (Carney et al. 2001; Carney, Latham & Laird 2005; Beers et al. 2007).

Dwarf spheroidal galaxies (dSphs) seem natural places to search for BSSs. Mateo et al. (1991) and Mateo, Fischer & Krzeminski (1995) first indicated the existence of a large number of stars brighter than the turn-off mass in the Sextans dSph. Mateo et al. (1995) suggested that these stars might be ordinary MS stars substantially younger than the bulk of the other stars. BSS candidates have been found in varying numbers in most dSphs, such as Sculptor (e.g. Hurley-Keller, Mateo & Grebel 1999; Monkiewicz et al. 1999), Draco (Aparicio, Carrera & Martínez-Delgado 2001, hereafter A01) and Ursa Minor (Carrera et al. 2002, hereafter C02).

The issue of whether these stars are young or BSSs has not been quantitatively addressed because there were not suitable models of BSS formation with predictive power with which to compare the observations. This also means that our proper understanding of the star formation history of these 'predominantly old' dSphs remains in doubt. Has there actually been low-level star formation in the last 8–10 Gyr in these galaxies or can they really be considered 'fossil' galaxies? Thus, in order to reconstruct the star formation history of dSphs, it is crucial to understand whether the observed BSS candidates are true BSSs rather than younger stars.

A second unsolved question about BSSs is their formation mechanism itself. BSSs are believed to have been somehow refuelled with hydrogen after the MS phase. However, the refuelling mechanism is still unknown. It has been proposed (McCrea 1964) that mass transfer in isolated binaries can lead to the formation of BSSs. On the other hand, BSSs could be the products of stellar collisions, occurring during (or triggered by) three- and four-body

⋆E-mail: mapelli@physik.unizh.ch

encounters (Davies, Benz & Hills 1994; Sigurdsson, Davies & Bolte 1994; Lombardi et al. 2002). In the first case, i.e. mass-transfer BSSs (MT-BSSs), BSSs can form if binaries are allowed to quietly evolve until they start the mass-transfer phase. This implies that the local density should not be too high, otherwise gravitational interactions will perturb the mass transfer. In the second case, i.e. collisionally born BSSs (COL-BSSs), the density must be sufficiently high to guarantee a short collision time-scale.

In globular clusters both processes might occur, as in the high-density core we find the perfect conditions for COL-BSS formation, while in the periphery MT-BSSs can originate from isolated binary evolution. In some circumstances, the features of the observed BSS population can be explained only by invoking a joint contribution by these mechanisms (Leonard 1989; Fusi Pecci et al. 1992; Bailyn & Pinsonneault 1995; Ferraro et al. 1997; Sills & Bailyn 1999; Hurley et al. 2001). For example, in some globular clusters the BSS radial distribution is bimodal (Ferraro et al. 1993, 1997; Zaggia et al. 1997; Ferraro et al. 2004; Sabbi et al. 2004), with a central peak, a minimum at intermediate radii, and a further rise at the periphery. Dynamical simulations by Mapelli et al. (2004, 2006, hereafter M04, M06, respectively) showed that this bimodal distribution can be reproduced only by requiring the central BSSs to be mainly COL-BSSs, and the peripheral BSSs to be MT-BSSs. Also, the luminosity function of BSSs in some globular clusters (Bailyn & Pinsonneault 1995; Sills & Bailyn 1999; Sills et al. 2000; Ferraro et al. 2003; Monkman et al. 2006) suggests the coexistence of COL-BSSs and MT-BSSs.

In dSphs, the collisional formation of BSSs should be impossible, as the central density of these galaxies never reaches sufficiently high values to allow stellar encounters. Thus, we expect BSSs in dSphs to be solely MT-BSS type.

In this paper, we seek to quantify the potential BSS population characteristics in dSphs and thereby learn more about BSS formation and evolution, and also about the star formation history in dSphs. First of all, we check whether the main characteristics (such as radial and luminosity distribution) of BSS candidates in dSphs are more consistent with those predicted by theoretical models of BSSs, or if they are more similar to MS young stars. At the same time, we would like to test whether the proposed formation mechanisms for BSSs also work in dSphs, i.e. whether the BSS candidates in dwarf galaxies can be connected with MT-BSSs.

We focus on the BSS population of two dSphs, Ursa Minor and Draco (see Table 1). These are among the faintest and most diffuse dwarfs in the Local Group (Irwin & Hatzidimitriou 1995, hereafter IH95; Mateo 1998). They also appear to be among the most dark matter dominated objects we know about (Kleyna et al. 2003; Wilkinson et al. 2004). Ursa Minor and Draco are also among those dSphs of the Local Group where star formation appeared to cease early on ($\gtrsim$8$-$10 Gyr ago; see Mateo 1998; Hernandez, Gilmore & Valls-Gabaud 2000; A01; C02; Bellazzini et al. 2002). In both these galaxies, a significant number of BSS candidates have been detected (A01; C02). If the observed BSS candidates in these two dSphs can be explained as young MS stars, the existence of BSSs in dwarf galaxies can probably be safely rejected. However, if instead these stars do behave like authentic BSSs, then Ursa Minor and Draco should be really considered two 'fossil' galaxies, where star formation indeed completely stopped many Gyr ago. Furthermore, by studying such diffuse systems we can also learn about the properties of BSSs in a much less dense environment than a globular cluster.

In Section 2, we present the data on which our analysis is based. In Section 3, we discuss the observational features of BSS candidates, with particular emphasis on the luminosity function and radial distribution characteristics. In Section 4, we describe our dynamical simulations and compare the results with observations. A comparison with previous work on BSS candidates in dwarf galaxies and globular clusters is presented in Section 5. Finally, in Section 6 we present our conclusions.

2 THE DATA

2.1 INT/WFC survey data

The Isaac Newton Telescope (INT) Wide Field Camera (WFC) is a mosaic of four 4 k $\times$ 2 k EEV chips, offering a field of view of $\sim$0.29 deg^2. It is mounted in the prime focus of the 2.5-m Isaac Newton Telescope on La Palma. The V'-band (Harris filter) and i'-band (SDSS-like)[1] data extend beyond the tidal radius in both Draco and Ursa Minor (see the upper panels of Fig. 1). They were taken as part of the INT Wide Field Survey (McMahon et al. 2001) during 2002 with an average seeing of 1 arcsec and in generally photometric conditions. The images were processed in the standard way with the INT WFC pipeline (Irwin & Lewis 2001). The two-dimensional instrumental signature removal includes provision for non-linearity correction at the detector level, bias and overscan correction prior to trimming to the active detector areas, flat-fielding and fringe removal in the i' band.

Catalogue generation follows the precepts outlined by Irwin (1985, 1996) and includes the facility to automatically track any background variations on scales of typically 20–30 arcsec, detect and deblend images or groups of images, and parametrize the detected images to give various (soft-edged) aperture fluxes, position and shape measures. The generated catalogues start with an approximate World Coordinate System (WCS) defined by the known telescope and camera properties (e.g. WCS distortion model) and are then progressively refined using all-sky astrometric catalogues [e.g. United States Naval Observatory (USNO), catalogue of astrometric standards, Automated Plate Measuring (APM) catalogue, Two Micron All Sky Survey (2MASS)] to give internal precision generally better than 0.1 arcsec and global external precision of 0.25 arcsec or better. These latter numbers are solely dependent on the accuracy of the astrometric catalogues used in the refinement.

All catalogues for all CCDs for each pointing are then processed using the image shape parameters for morphological classification in the main categories: stellar; non-stellar; noise-like. A sampled curve-of-growth for each detected object is derived from a series of aperture flux measures as a function of radius. The classification is then based on comparing the curve-of-growth of the flux for each detected object with the well-defined curve-of-growth for the general stellar locus. This latter is a direct measure of the integral of the point spread function (PSF) out to various radii and is independent of magnitude, if the data are properly linearized, and if saturated images are excluded. The average stellar locus on each detector is clearly defined and is used as the basis for a null hypothesis stellar test for use in classification. The curve-of-growth for stellar images is also used to automatically estimate frame-based aperture corrections for conversion to total flux.

The photometric standards observed during the run (mainly Landolt 1992, and spectrophotometric standards) are automatically located in a standards database and used to estimate the zero-point

[1] For filter responses, see http://www.ast.cam.ac.uk/$\sim$wfcsur/technical/filters/

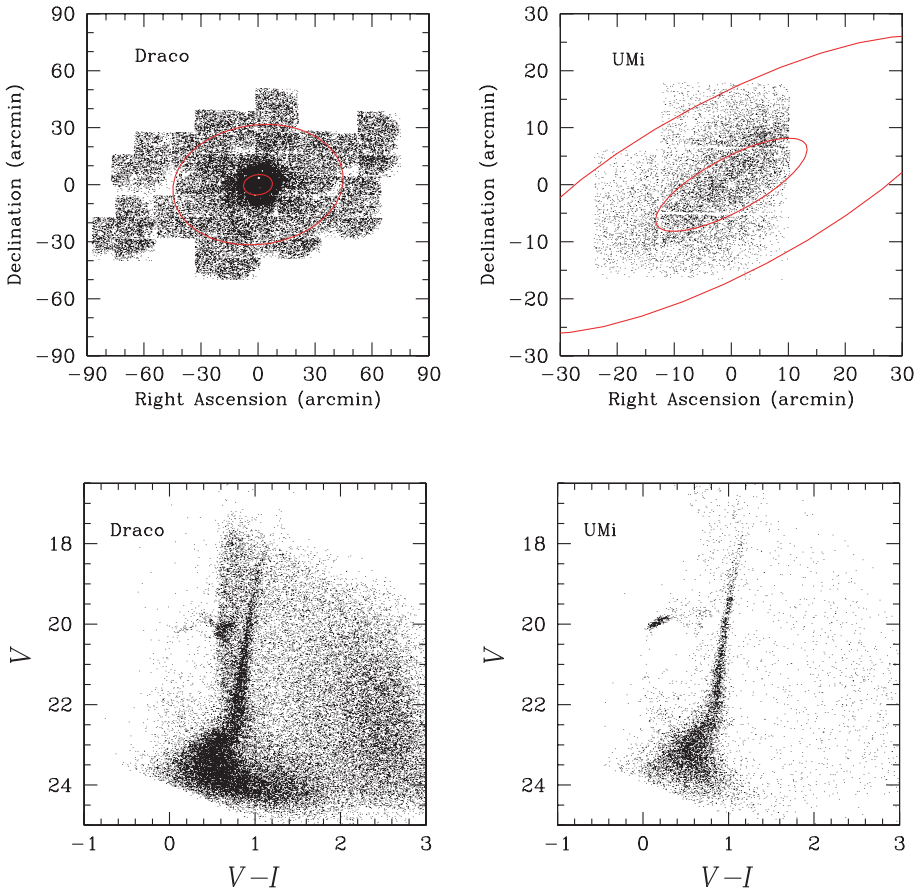

Figure 1. Upper panel: right ascension and declination of the stars imaged in Draco (left-hand panel) and Ursa Minor (right-hand panel). The concentric ellipses indicate tidal and core radii (r_t and r_c; the adopted values are listed in Table 1). In both cases, the origin of the axes coincides with the centre of the observed galaxy. Bottom panel: CMDs of Draco (left-hand panel) and Ursa Minor (right-hand panel).

in each passband for every pointing containing any of these standards. The trend in the derived zero-points is then used to assign a photometric quality index for each night and also as a first pass estimate for the magnitude calibration for all the observations.

Various quality control plots are generated by the pipeline and these are used to monitor characteristics such as the seeing, the average stellar image ellipticity (to measure trailing), the sky brightness and sky noise, the size of aperture correction for use with the 'optimal' aperture flux estimates (here 'optimal' refers to the well-known property that soft-edged apertures of roughly the average seeing radius provide close to profile fit accuracy; e.g. Naylor 1998).

The 'optimal' catalogue fluxes for the V', i' filters for each field are then combined to produce a single matched catalogue for each pointing and the overlaps between pointings are used to cross-calibrate all the catalogues to a common system with typical accuracy 1–2 per cent across the survey region. The final step is to produce a unique catalogue for the whole region by removing spatially coincident (within 1 arcsec) duplicates.

As a final stage, the data are converted[2] from the instrumental WFC V' and i' passbands to the Johnson–Cousins V, I system to obtain the standard CMD shown in the lower panel of Fig. 1.

[2] For details of the conversion see http://www.ast.cam.ac.uk/~wfcsur/technical/photom/

2.2 Stellar population selection criteria

From these data, we selected three different populations: BSSs, red giant branch (RGB) and horizontal branch (HB) stars. The last two populations are considered good tracers of the overall light from the galaxy, and we use them as a comparison for BSS distributions. For all these populations, we adopt more conservative selection criteria with respect to previous works (see e.g. A01; C02; Lee et al. 2003, hereafter L03) in order to minimize the contamination by stars of different populations. The regions of the CMD we associate with BSSs, RGB and HB stars are indicated in Fig. 2 as boxes 1, 2 and 3, respectively. In particular, for BSSs we chose the V and (V-I) range to be (i) sufficiently above the turn-off, in order to avoid contamination from the MS, (ii) blue-ward of the RGB, avoiding not only contamination from these stars but, especially, also the region of the CMD most affected by the Galactic foreground, and (iii) red-ward of a possible faint extension of the very blue extended HB.

Furthermore, we select a narrow strip of RGB stars (box 2) to limit the effect of binaries and errors in magnitude. The large number of RGB stars in the sample allows us this conservative choice. Finally, the HB region is divided in two different regions, approximately corresponding to the red HB (RHB) and the blue HB (BHB). As it has already been noted (C02), the HB in Ursa Minor is substantially bluer than in Draco.

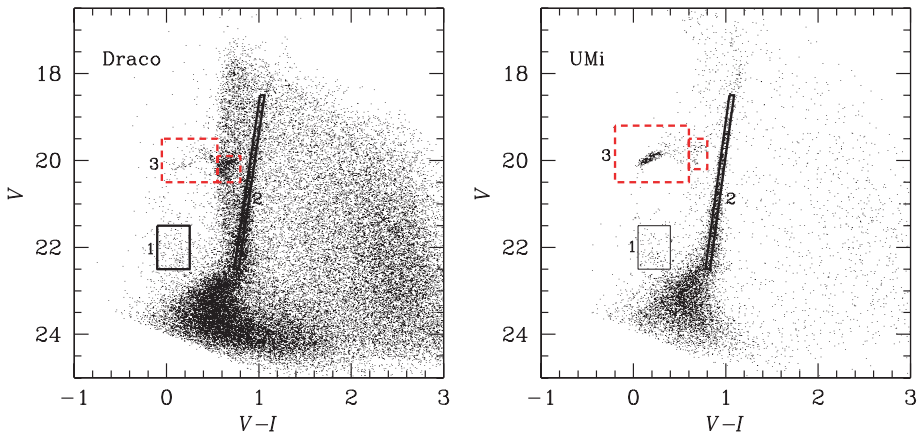

Figure 2. CMD of Draco (left-hand panel) and Ursa Minor (right-hand panel) with stellar population selection boxes overlaid. Boxes indicated by the solid line and labelled as 1 and 2 are the BSSs and RGB stars, respectively. Boxes indicated by the dashed line and labelled as 3 are the HB stars, divided as blue and red.

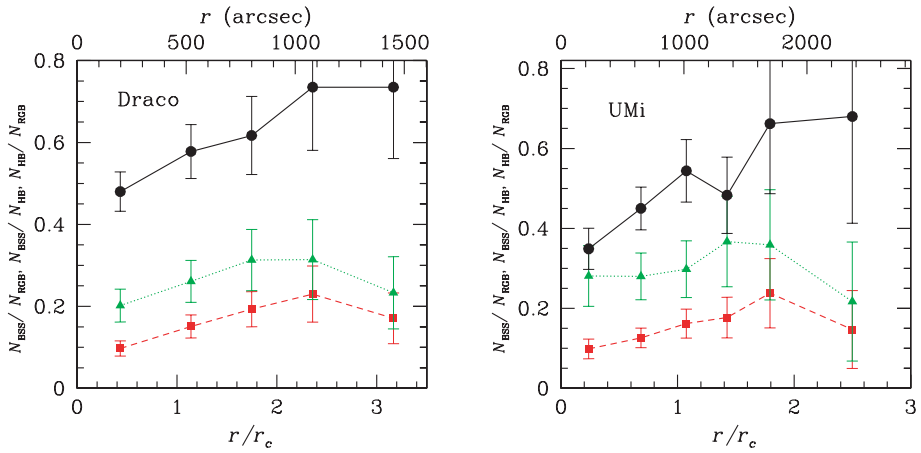

Figure 3. Observed relative frequency of BSSs normalized to RGB stars (filled squares connected by dashed line) and HB stars (filled triangles connected by dotted line). Observed relative frequency of HB stars normalized to RGB stars (filled circles connected by solid line). Left-hand panel refers to Draco and right-hand panel to Ursa Minor.

We also checked that these more restrictive selection criteria do not significantly affect our results both for the radial and for the luminosity distribution (see next section for the comparison with L03).

3 OBSERVATIONAL PROPERTIES OF BSS CANDIDATES

After accounting for the foreground and background contamination[3] in our data (see Appendix A for the details), we can extract information about the radial[4] distribution of different populations of stars as well as about their luminosity distribution. Both these quantities are important to understand the behaviour of BSS candidates [see e.g. M06 for the radial distribution and Monkman et al. (2006) for the luminosity].

3.1 Radial distributions

Fig. 3 shows the radial distribution of the ratio between the number of BSSs ($N_{\rm BSS}$) and that of RGB ($N_{\rm RGB}$) and of HB stars ($N_{\rm HB}$). The radial distribution of $N_{\rm HB}$ with respect to $N_{\rm RGB}$ is also shown in Fig. 3. The quantities used in Fig. 3 are listed in Tables 2 and 3 for Draco and Ursa Minor, respectively.

The behaviour of these three relative frequencies is qualitatively similar in Ursa Minor (right-hand panel) and Draco (left-hand panel).

From the shape of the distributions in Fig. 3, we can see that the BSS candidates appear to be slightly less concentrated than both HB and RGB stars. The relative frequency of BSSs is low especially within 1 $r_{\rm c}$, and there are hints of a maximum at a distance $1.5\,r_{\rm c} \lesssim r \lesssim 2.5\,r_{\rm c}$. The most remarkable feature of this distribution is the absence of a central peak in the relative BSS frequency, which is present in nearly every globular cluster.

[3] Our selection boxes are contaminated both by Milky Way stars in the foreground and by extragalactic objects (e.g. quasars and unresolved galaxies) in the background. Since the foreground component is generally dominant, in the rest of this paper we will refer to any type of contamination as 'foreground', unless the distinction is important.

[4] All the references to 'radii' in this paper mean *elliptical radii*. The elliptical radius of a point (x, y) is $r_{\rm ell}(x, y)^2 = x^2 + [y/(1 - e)]^2$, where e is the ellipticity of the considered galaxy, and the galaxy is assumed to be centred on the origin, with its major axis aligned with the x-axis.

The distributions of $N_{\rm BSS}/N_{\rm HB}$ and $N_{\rm BSS}/N_{\rm RGB}$ are marginally consistent with flat distributions. In fact, if we try to fit $N_{\rm BSS}/N_{\rm RGB}$ with a flat distribution, the minimum non-reduced χ^2 is 8.4 (corresponding to a level of the flat distribution equal to 0.129) and 4.9 (for a level of the flat distribution equal to 0.130), for Draco and Ursa Minor,[5] respectively. The resultant null hypothesis probability for a flat distribution is only $\sim$0.08 for Draco and $\sim$0.43 for Ursa Minor.

Similarly, to fit $N_{\rm BSS}/N_{\rm HB}$ with a flat distribution, the minimum non-reduced χ^2 is 2.6 (corresponding to a level of the flat distribution equal to 0.243) and 1.0 (for a level of the flat distribution equal to 0.288), for Draco and Ursa Minor, respectively. The resultant null hypothesis probability for a flat distribution is $\sim$0.63 for Draco and $\sim$0.96 for Ursa Minor.

We also checked the probability that $N_{\rm BSS}/N_{\rm RGB}$ and $N_{\rm BSS}/N_{\rm HB}$ are consistent with a distribution rising in the central bin and flat elsewhere.[6] For Draco, we found that this probability drops below 0.05 if the central bin is a factor of 1.00 (1.49) higher than the outer ones in the case of $N_{\rm BSS}/N_{\rm RGB}(N_{\rm BSS}/N_{\rm HB})$. For Ursa Minor, the probability drops below 0.05 if the central bin is a factor of 1.45 (2.42) higher than the outer ones in the case of $N_{\rm BSS}/N_{\rm RGB}(N_{\rm BSS}/N_{\rm HB})$. Then, we can conclude that the observed distribution of $N_{\rm BSS}/N_{\rm HB}$ and especially $N_{\rm BSS}/N_{\rm RGB}$ is hardly consistent with a central rise like the one we observe in most of globular clusters (M06).

If BSS candidates were young MS stars, we would expect them to be more concentrated than older stars, consistent with observations where metal-rich (younger) stars are typically more centrally concentrated than metal-poor (older) stars (e.g. Tolstoy et al. 2004; Battaglia et al. 2006).

Furthermore, the spatial distribution of BSS does not show the clumping which could be expected in the case of a young population (e.g. Fornax dSph; Battaglia et al. 2006). Thus, the observed radial distribution of BSS candidates suggests (even if it does not prove) that these stars are BSSs and not a young population.

Are these observed radial distributions consistent with models of BSS formation and evolution? According to the model by M04 and M06, most BSSs in the core of a dense host system form from collisions. A central peak in the relative BSS frequency is expected only if a sufficiently large number of COL-BSSs can form.

The absence of any central peak in Fig. 3 is consistent with this model. In fact, in dSphs the stellar density, even in the core, is so low that stellar collisions are unlikely to occur,[7] and COL-BSSs cannot form. The dearth of BSSs in the centre is also favoured by the inefficiency of dynamical friction in dSphs: even if BSSs have higher mass than both RGB and HB stars, it takes too long for them to sink to the centre.

Furthermore, M04 and M06 also predict that MT-BSSs (see Section 4) have a relative frequency that is almost flat in the centre and slightly rising in the periphery. This implies that BSS candidates in Draco and Ursa Minor do behave like MT-BSSs, whereas they are unlikely to be COL-BSSs.

We compared our definitions of BSSs and other populations with those used by L03 and tested the robustness of different choices. L03 adopt a wider definition of BSS, and normalize the frequency of BSSs to the number of sub-giant branch (SGB) stars. We used both our definition of BSSs and normalization to the RGB stars and the L03 definition adapted for the distances and reddenings of Draco/Ursa Minor, combined with a normalization to SGB stars. We do not observe any significant difference.

This suggests that our results are reasonably independent of the BSS selection criteria, and also of the stellar population we choose as a normalization control sample (HB, RGB or SGB).

In Fig. 3, it can also be seen that HB stars also seem to be slightly less concentrated than RGB stars. This again is consistent with trends seen in other dSph (Harbeck et al. 2002; L03; Tolstoy et al. 2004; Battaglia et al. 2006), suggesting that older populations tend to be less centrally concentrated. In particular, the blue old stellar populations (BHB, blue RGB, etc.) tend to be less concentrated than their red counterparts (RHB, red RGB, etc.). However, as in the case of $N_{\rm BSS}/N_{\rm HB}$ and $N_{\rm BSS}/N_{\rm RGB}$, $N_{\rm HB}/N_{\rm RGB}$ is also statistically consistent with a flat distribution.

3.2 Luminosity distribution

The luminosity distribution is another important indicator of BSS properties. Recent papers (Ferraro et al. 2003; Monkman et al. 2006) suggest a correlation between the brightness of BSSs and their radial distance from the centre of a globular cluster. Bright BSSs tend to be more concentrated than the faint ones. In turn, if the model of M04 and M06 is correct, such a correlation suggests that the centrally concentrated COL-BSSs tend to be brighter than MT-BSSs. This scenario makes sense, as COL-BSSs should conserve a large fraction of the mass of the colliding progenitors (Benz & Hills 1987, 1992; Sills et al. 2001; Freitag & Benz 2005), whereas the mass-transfer process is not as efficient (Pols & Marinus 1994; Tian et al. 2006).

In dSphs, where only MT-BSSs are likely to form, we do not expect to see a correlation between the brightness of BSSs and their radial position. This prediction is completely supported by the observed BSS luminosity distribution of Draco (Fig. 4, left-hand panel) and Ursa Minor (Fig. 4, right-hand panel). The open histograms in Fig. 4 show the total luminosity distribution, while the light and heavy hatched histograms show the luminosity distribution of BSSs which are located outside and within $r_{\rm c}$, respectively. According to the Kolmogorov–Smirnov (KS) test, the probability that light and heavy hatched histograms are drawn from the same distributions is $>$0.999 both for Draco and for Ursa Minor. Thus, there is no statistically significant difference between these distributions, indicating no dependence of the luminosity function on the radial distance. This fact is at odds with the findings by L03, who observe a correlation between the brightness of BSSs in Sextans and their radial distance. Since (as we checked) our luminosity distributions do not change by adopting the BSS selection criteria by L03, we suggest that this is due to an intrinsic difference between Sextans and Draco/Ursa Minor (see Section 5).

4 THE SIMULATIONS

The data presented in the previous sections show that BSS candidates in Draco and Ursa Minor behave like MT-BSSs. As a further

[5] The data points used in the χ^2 analysis are five for Draco and six for Ursa Minor (see Fig. 3). There is one parameter, i.e. the level of the flat distribution.

[6] For this analysis, we have two parameters: the level of the central bin and the level of the flat distribution for the other bins.

[7] The collision rate, defined as (Davies, Piotto & De Angeli 2004) $\Gamma \sim N_{\rm c}\, n_{\rm c}\, \Sigma_{\rm coll}\, \sigma_{\rm c}$ (where $\Sigma_{\rm coll}$ is the collision cross-section, $N_{\rm c}$ the number of stars in the core, $n_{\rm c}$ and $\sigma_{\rm c}$ the stellar number density and velocity dispersion in the core), is more than a factor of 10^5 smaller in dSphs than in globular clusters.

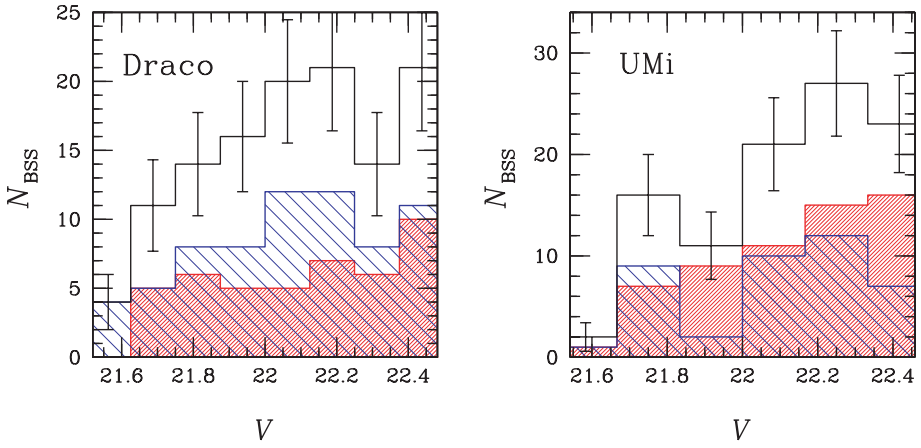

Figure 4. Luminosity distribution of BSSs in Draco (left-hand panel) and Ursa Minor (right-hand panel). The empty histogram represents the entire sample of BSSs and the error bars show the Poissonian error. The lightly hatched (heavily hatched) histogram represents BSSs with radial position $r > r_c (r < r_c)$.

Table 1. Galaxy parameters.

Galaxy	d^a (kpc)	$r_c{}^b$ (arcsec)	$r_t{}^b$ (arcsec)	σ_c (km s^{-1})^c	n_c (stars pc^{-3})^d	$W_0{}^e$	c^e	Ellipticity^b
Draco	83	457.8	2706	10.5	3.2×10^{-3}	2.0	0.76	0.29
Ursa Minor	76	948	3036	12.5	10^{-3}	0.45	0.52	0.56

[a]We assume distance moduli of 19.60 (Draco) and 19.41 (Ursa Minor) (see Appendix B); [b]Core radius (r_c), tidal radius (r_t) and ellipticity are from Ségall et al. (2007) and from IH95 for Draco and Ursa Minor, respectively. [c]Core velocity dispersion of the dSph, from Wilkinson et al. (2004). [d]Core density (n_c)of the dSph, derived from our data. [e]Central adimensional potential (W_0) and concentration [$c = \log(r_c/r_t)$] are derived from our simulations. c is consistent with IH95 for Ursa Minor and with Ségall et al. (2007) for Draco.

check, we ran for Draco and Ursa Minor the same kind of dynamical simulations that were performed by M04 and M06 for BSSs in globular clusters.

4.1 Method

We adopt the upgraded version of the code by Sigurdsson & Phinney (1995) already described in M04 and M06. The code integrates the dynamics of BSSs, under the influence of the galactic potential, of dynamical friction (using Chandrasekhar formula) and of distant encounters with other stars. Also three-body encounters are implemented in the code, but they are unimportant in the runs for dSphs.

The potential of the host galaxy is represented by a time-independent multimass King model. The classes of mass are the same as in M04, and the assumed turn-off mass is $0.8\,M_\odot$. To calculate the potential, we input the observed core density (n_c) and velocity dispersion (σ_c) of Draco and Ursa Minor (the adopted values are listed in Table 1), and we modify the value of the central adimensional potential, W_0 (defined in Sigurdsson & Phinney 1995), until we reproduce the concentration and the density profile of the galaxy under consideration. In Fig. 5, the density profiles of the best-fitting King models are compared with the data of IH95. As expected, the best-fitting value of W_0 is a factor of 5–20 lower than the common values assumed in globular clusters.

BSSs are generated with a given position, velocity and mass. Initial positions are randomly chosen according to a probability distribution homogeneous in the radial distance from the centre. This means that BSSs are initially distributed according to an isothermal sphere, as we expect for MT-BSSs (see M04 and M06). The minimum and the maximum value of the distribution of initial radial distances, r_{min} and r_{max}, have been tuned in order to find the best-fitting simulation (Tables 4 and 5 report the most significant runs and their parameters for Draco and Ursa Minor, respectively).

Table 2. Number counts for Draco.

r (arcsec)^a	$N_{BSS}{}^b$	$\epsilon_{BSS}{}^c$	$N_{RGB}{}^b$	$\epsilon_{RGB}{}^c$	$N_{HB}{}^b$	$\epsilon_{HB}{}^c$
198	30.8 (31)	5.6	316 (319)	17.9	152 (155)	12.5
522	33.5 (34)	5.8	222 (227)	15.1	128 (134)	11.7
800	25.1 (26)	5.1	130 (139)	11.8	80.3 (94)	10.1
1080	15.1 (16)	4.0	65.3 (75)	8.7	48.0 (56)	7.7
1450	11.5 (14)	3.8	67.2 (93)	9.9	49.3 (72)	9.2

[a]Centre of the annulus. [b]The value out of (in) the parenthesis is after (before) the subtraction of the foreground. [c]Poissonian error plus a term accounting for foreground subtraction.

Table 3. Number counts for Ursa Minor.

r (arcsec)^a	$N_{BSS}{}^b$	$\epsilon_{BSS}{}^c$	$N_{RGB}{}^b$	$\epsilon_{RGB}{}^c$	$N_{HB}{}^b$	$\epsilon_{HB}{}^c$
225	17.9 (18)	4.2	182 (183)	13.5	63.5 (64)	8.0
650	29.8 (30)	5.5	237 (239)	15.5	106.0 (110)	10.6
1020	23.7 (24)	4.9	146 (149)	12.2	79.5 (84)	9.3
1350	14.7 (15)	3.9	82.8 (86)	9.3	40.0 (41)	6.4
1700	9.7 (10)	3.2	40.8 (44)	6.6	27.0 (29)	5.5
2370	2.8 (3)	1.7	19.1 (21)	4.6	13.0 (15)	4.0

[a]Centre of the annulus. [b]The value out of (in) the parenthesis is after (before) the subtraction of the foreground. [c]Poissonian error plus a term accounting for foreground subtraction.

Table 4. Simulation parameters and χ^2 for Draco.

Run	$r_{\rm min}/r_{\rm c}$	$r_{\rm max}/r_{\rm c}$	$v_{\rm kick}/\sigma_{\rm c}$	$t_{\rm last}$ (Gyr)	$m_{\rm BSS}$ ($M_\odot$)	$\chi^2_{\rm RGB}$	$\chi^2_{\rm HB}$
A1	0.8	3.5	0	2	1.3	0.31	0.26
A2	0.8	3.5	0	1	1.3	0.54	0.47
A3	0.8	3.5	0	4	1.3	0.58	0.49
A4	0.8	3.5	0	10	1.3	0.64	0.54
B1	0.	3.5	0	2	1.3	4.51	4.08
B2	0.2	3.5	0	2	1.3	2.46	2.23
B3	0.5	3.5	0	2	1.3	0.62	0.60
B4	1.0	3.5	0	2	1.3	1.09	0.94
C1	0.8	4.5	0	2	1.3	4.02	3.64
C2	0.8	3.0	0	2	1.3	1.89	1.72
C3	0.8	2.5	0	2	1.3	7.03	6.47
D1	0.	4.5	0	2	1.3	2.74	2.47
D2	0.	3.0	0	2	1.3	8.67	7.89
E1	0.8	3.5	0	2	1.1	0.31	0.26
E2	0.8	3.5	0	2	1.5	0.56	0.47
F1	0.8	3.5	1.	2	1.3	0.85	0.73

$\chi^2_{\rm RGB}$ ($\chi^2_{\rm HB}$) indicates the χ^2 of the $N_{\rm BSS}/N_{\rm RGB}$($N_{\rm BSS}/N_{\rm HB}$) distribution. The reported values of $\chi^2_{\rm RGB}$ and $\chi^2_{\rm HB}$ are not reduced and have been calculated on the basis of five data points.

Table 5. Simulation parameters and χ^2 for Ursa Minor.

Run	$r_{\rm min}/r_{\rm c}$	$r_{\rm max}/r_{\rm c}$	$v_{\rm kick}/\sigma_{\rm c}$	$t_{\rm last}$ (Gyr)	$m_{\rm BSS}$ ($M_\odot$)	$\chi^2_{\rm RGB}$	$\chi^2_{\rm HB}$
A1	0.5	1.9	0	2	1.3	0.42	0.36
A2	0.5	1.9	0	1	1.3	0.32	0.28
A3	0.5	1.9	0	4	1.3	0.20	0.17
A4	0.5	1.9	0	10	1.3	0.34	0.29
B1	0.0	1.9	0	2	1.3	1.68	1.50
B2	0.2	1.9	0	2	1.3	0.58	0.53
B3	0.8	1.9	0	2	1.3	1.93	1.61
B4	1.0	1.9	0	2	1.3	3.51	2.95
C1	0.5	3.0	0	2	1.3	18.07	16.06
C2	0.5	2.5	0	2	1.3	4.79	4.24
C3	0.5	1.0	0	2	1.3	6.99	6.21
D1	0.0	3.0	0	2	1.3	12.60	11.29
D2	0.0	1.5	0	2	1.3	5.53	4.89
E1	0.5	1.9	0	2	1.1	0.42	0.36
E2	0.5	1.9	0	2	1.5	0.43	0.36
F1	0.5	1.9	1	2	1.3	2.67	2.33

Note. $\chi^2_{\rm RGB}$ ($\chi^2_{\rm HB}$) indicates the χ^2 of the $N_{\rm BSS}/N_{\rm RGB}$($N_{\rm BSS}/N_{\rm HB}$) distribution. The reported values of $\chi^2_{\rm RGB}$ and $\chi^2_{\rm HB}$ are not reduced and have been calculated on the basis of six data points.

Initial velocities are generated from the distributions described in Sigurdsson & Phinney (1995). In most runs, no initial kicks are given to BSSs because they are expected to be MT-BSSs. We also made some (physically unrealistic) check run, where a kick velocity ($v_{\rm kick}$) is given to BSSs born inside the core.

In most of the runs, the mass of the BSSs is assumed to be $m_{\rm BSS} = 1.3\,M_\odot$. We made check runs with masses in the range from 1.1 to $1.5\,M_\odot$ (higher masses are unlikely, at least for some globular clusters; see Ferraro et al. 2004, 2006). This range of masses is also consistent with the isochrones for our data of Draco and Ursa Minor (see Appendix B).

Each BSS is evolved for a time t, randomly selected from a homogeneous distribution between $t = 0$ and $t = t_{\rm last}$. The parameter $t_{\rm last}$ represents the lifetime of BSSs (see M04, M06). We made runs with $t_{\rm last} = 1, 2, 4, 10$ Gyr.

4.2 Comparison with observations

We ran different simulations, adopting different masses and lifetimes for BSSs, and varying the interval $[r_{\rm min}, r_{\rm max}]$ where MT-BSSs are allowed to form. For each of them, we obtain the distributions $N_{\rm BSS}/N_{\rm RGB}$ and $N_{\rm BSS}/N_{\rm HB}$, and calculate their χ^2 ($\chi^2_{\rm RGB}$ and $\chi^2_{\rm HB}$, respectively) with respect to observations.

From the χ^2 analysis (Tables 4 and 5), it appears that the lifetime of BSSs, $t_{\rm last}$, does not affect the results: runs A1, A2, A3 and A4, which differ only for $t_{\rm last}$, have $\chi^2_{\rm RGB} \sim \chi^2_{\rm HB} \sim 1$, both in Draco and in Ursa Minor. Then, in the case of dSphs, our simulations cannot constrain the age of BSSs. The reason is that dSphs are dynamically 'quiet' environments, where, due to the low density, both dynamical friction and close interactions are inefficient.

On the other hand, if BSSs burn a tiny amount of hydrogen, acquired from the companion stars, they are expected to be relatively short lived. Thus, the run with $t_{\rm last} = 10$ Gyr (A4 for both Draco and Ursa Minor) is likely unrealistic. In the following, we will consider $t_{\rm last} = 2$ Gyr as the fiducial value, for analogy with the findings of M04 and M06 for globular clusters, and because an age of about 2 Gyr is suggested also by isochrones (see Appendix B).

Also, the mass of the BSS is not a crucial parameter: runs A1, E1 and E2, which differ only in the BSS mass, have $\chi^2_{\rm RGB} \sim \chi^2_{\rm HB} \lesssim 1$. In most of the runs, we assume as fiducial value $m_{\rm BSS} = 1.3\,M_\odot$. Masses larger than $m_{\rm BSS} \sim 1.4{-}1.5\,M_\odot$ tend to be discarded by observations, both in our data (see Appendix B) and in globular clusters (Ferraro et al. 2006).

The parameters which mainly affect our results are the lower and upper limit of the initial radial position distribution ($r_{\rm min}$ and $r_{\rm max}$). We remind that initial positions in such simulations represent the point where a binary which is undergoing mass transfer turns into a BSS.

The best-fitting value for $r_{\rm min}$ is similar for Draco and Ursa Minor, and is equal to 0.8 $r_{\rm c}$ and 0.5 $r_{\rm c}$, respectively. All the values of $r_{\rm min}$ from 0 to $\sim$1 $r_{\rm c}$ give acceptable χ^2 (see e.g. runs B1–B4 both for Draco and for Ursa Minor).

The best-fitting $r_{\rm max}$ (expressed in terms of $r_{\rm c}$) is a factor of $\sim$2 larger for Draco (3.5 $r_{\rm c}$) than for Ursa Minor (1.9 $r_{\rm c}$). Indeed, it is possible to reproduce Draco BSSs, recovering an acceptable χ^2, also with $2.5 \leqslant r_{\rm max}/r_{\rm c} \leqslant 4.5$, whereas in the case of Ursa Minor $r_{\rm max} > 2.5\,r_{\rm c}$ and $r_{\rm max} < r_{\rm c}$ are inconsistent with observations (see e.g. runs C1–C3 both for Draco and for Ursa Minor).

This discrepancy might be due only to the different normalization. In fact, the core radius of Ursa Minor is approximately twice as large as that of Draco. In physical units, the best fits are $r_{\rm min} \sim 370$ and $r_{\rm max} \sim 1600$ arcsec (150 and 640 pc) for Draco, and $r_{\rm min} \sim 470$ and $r_{\rm max} \sim 1800$ arcsec (160 and 620 pc) for Ursa Minor.

The runs labelled as F1 in the case of both Draco and Ursa Minor have been set up by taking the best-fitting parameters (runs labelled as A1) and adding a small kick velocity $v_{\rm kick} = \sigma_{\rm c}$ to BSSs born inside $r_{\rm c}$. This check is physically unrealistic, as the natal kick is associated with COL-BSSs, which cannot form in dSphs. Interestingly, the χ^2 is quite good in both cases. However, we note that more than 10 per cent of BSSs are 'spuriously' ejected in these runs.

Figs 6 and 7 compare our fiducial model (run A1) with observations, for Draco and Ursa Minor, respectively. The good agreement with data is evident: the model has $\chi^2_{\rm RGB} = \chi^2_{\rm HB} \sim 0.3$ for Draco (five data points) and $\chi^2_{\rm RGB} = \chi^2_{\rm HB} \sim 0.4$ for Ursa Minor (six data points).

In summary, the dynamical simulations reproduce the observations very well for all the possible MT-BSS masses and lifetimes

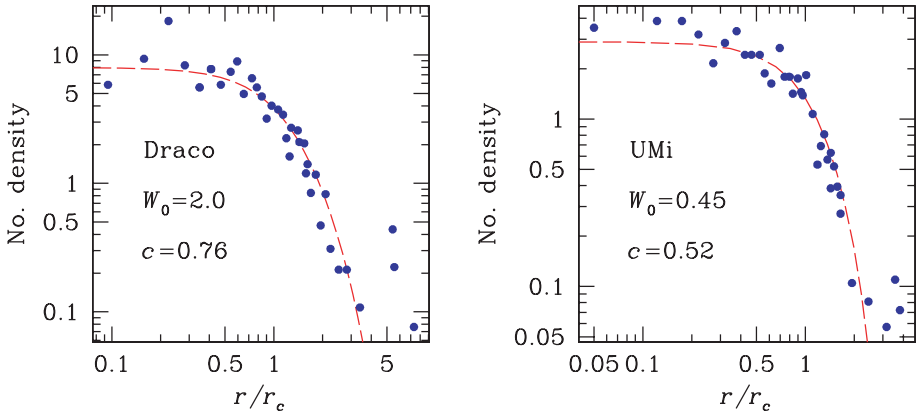

Figure 5. Surface density profile of Draco (left-hand panel) and Ursa Minor (right-hand panel). The number density is given in stars per arcmin^2. The filled circles are data points from IH95. The dashed line is the best-fitting simulation.

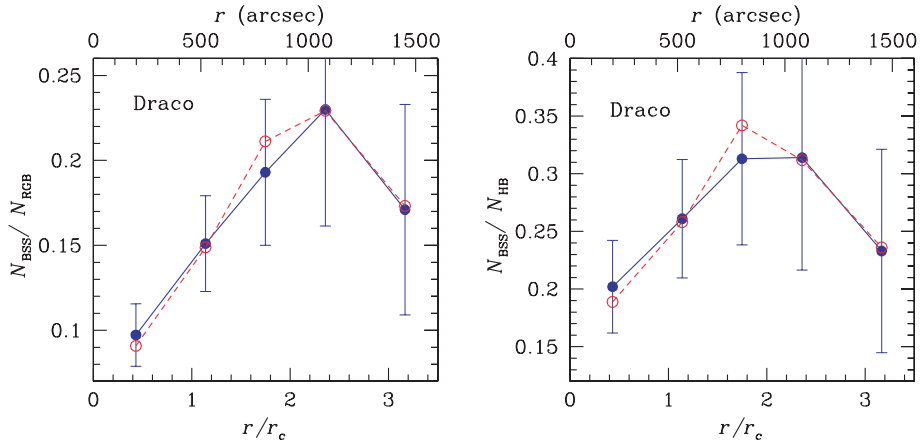

Figure 6. Relative frequency of BSSs normalized to RGB (left-hand panel) and HB stars (right-hand panel) in Draco. The filled circles connected by the solid line are the measurements (the same as in Fig. 3). The open circles connected by the dashed line are the fiducial model (run A1).

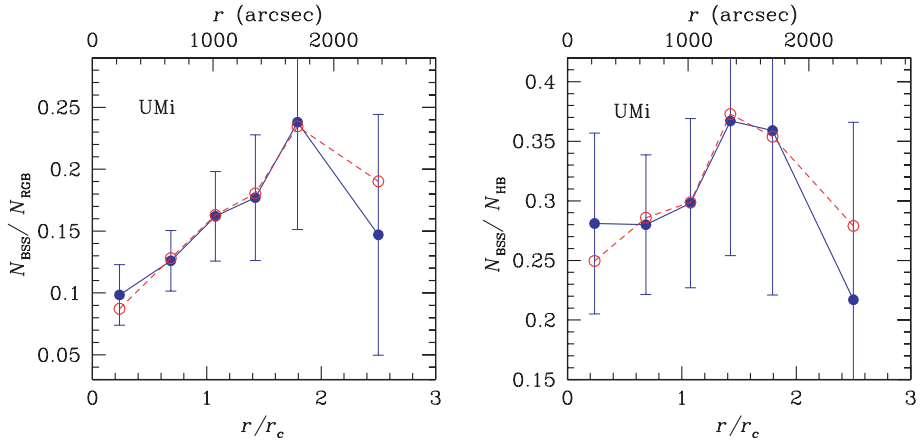

Figure 7. Relative frequency of BSSs normalized to RGB (left-hand panel) and HB stars (right-hand panel) in Ursa Minor. The filled circles connected by the solid line are the measurements (the same as in Fig. 3). The open circles connected by the dashed line are the fiducial model (run A1).

in the range allowed by the models. The best fit is achieved for the model with $r_{min} = 0.8\,r_c$ and $r_{max} = 3.5\,r_c$ for Draco, and with $r_{max} = 0.5\,r_c$ and $r_{max} = 1.9\,r_c$ for Ursa Minor. However, all r_{min} from 0 to r_c are acceptable, as well as all the r_{max} within $\approx 0.5\,r_c$ from the best-fitting value. Thus, BSS candidates are consistent with a population initially distributed in an isothermal sphere between the centre of the galaxy and the tidal radius. This result agrees with the model of BSS formation from mass-transferring binaries, and hints that BSS candidates in Draco and Ursa Minor are real MT-BSSs.

5 COMPARISON WITH OTHER GALAXIES AND GLOBULAR CLUSTERS

BSSs have been observed in most globular clusters and at least in four dSphs: Draco (A01), Sculptor (Hurley-Keller et al. 1999), Sextans (L03) and Ursa Minor (C02). It is instructive to compare our findings with previous papers on both dSphs and globular clusters.

5.1 Comparison with other dSphs

Previous studies of Draco (A01) and Sculptor (Hurley-Keller et al. 1999) do not report information about the radial distribution or the luminosity of BSSs. However, Hurley-Keller et al. (1999) calculate the ratio $N_{\rm BSS}/N_{\rm SGB}$ in the inner region of the galaxy (a box of 15 × 15 arcmin^2 centred on the centre of the galaxy) and in the outer one. They find that this ratio changes only by a factor of 1.5 between the inner and the outer region, suggesting that BSSs are not very concentrated.

On the other hand, A01 suggest that BSS candidates in Draco are consistent with a population of intermediate-age stars. In fact, they find a 'red clump' population in the CMD diagram, which might support this interpretation. This hypothesis cannot be ruled out also in the case of our data (see discussion in Appendix B).

C02 analysed the ratio of the number of 'blue plume' stars (corresponding to a wider definition of BSS) and the number of HB stars as a function of radius (see their fig. 10) in Ursa Minor. They find an almost flat distribution, whereas we note a small rise in the relative frequency of BSSs around 1.4 $r_{\rm c}$, but given the large error bars, our distribution is also consistent with a flat one ($\chi^2 \sim 1$ with six data points). However, not only was the definition of BSS in C02 different, but also the observed photometric bands: C02 build their CMD by plotting a 'V' magnitude, which is actually the average between R and B magnitudes, versus the $(B - R)$ colour. Thus, our results and those of C02 are not directly comparable. The most important fact is that both C02 and our findings suggest that there is no central peak of BSSs in Ursa Minor.

As we already mentioned in Section 3, L03 show both the radial and the luminosity distribution of BSS candidates in Sextans. Furthermore, their data are more easily comparable with ours, as they use the same filters. However, even if we adopt the same definition of BSS and the same normalization as L03, we do not find in either Draco or Ursa Minor any correlation between the brightness and the radial position of the BSSs, unlike that reported by L03 in Sextans. This discrepancy is unlikely due to the lack of statistics in our data, because, when we adopt the same selection criteria as L03, the number of BSSs rises to 198 in Draco and 212 in Ursa Minor, which is quite close to the sample of L03 (i.e. ∼230 BSSs).

The difference here might be due to statistical fluctuations, or could simply be connected with the intrinsic properties of Sextans, which are quite different from those of Draco and Ursa Minor. For example, Sextans has a higher concentration index ($c \sim 1$) with respect to both Draco and Ursa Minor, and it is very extended ($r_{\rm c} = 16.6$ arcmin and $r_{\rm t} = 160$ arcmin, IH95). L03 show the radial distribution of BSSs only within ∼1.1 $r_{\rm c}$, without information about external BSSs. It has recently been claimed that the centre of Sextans contains a kinematically distinct stellar population, which might be associated with a star cluster (Kleyna et al. 2004; but also see Walker et al. 2006). Indeed, the correlation between position and brightness of BSSs could be explained by invoking the presence of a star cluster. In this case, the bright BSSs, more concentrated towards the centre, could be COL-BSSs or even young stars formed in the star cluster; whereas the faint BSSs are MT-BSSs, like those in Draco and Ursa Minor. (We note that the distribution of faint BSSs alone in Sextans is quite similar to the distribution of the entire BSS sample in Draco and Ursa Minor.)

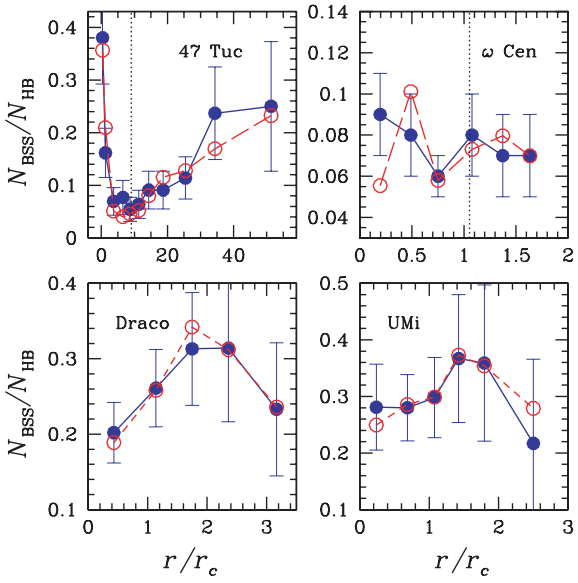

Figure 8. From left- to right-hand side and top to bottom: relative frequency of BSSs normalized to HB stars in 47 Tucanae, ω Centauri, Draco and Ursa Minor. Filled (open) circles connected by the solid (dashed) line are the observations (best-fitting simulations). The dotted vertical line in 47 Tucanae and ω Centauri panels indicate $r_{\rm av}$. The data and models for Draco and Ursa Minor are the same as in Figs 6 and 7, respectively. The data for 47 Tucanae and ω Centauri are from Ferraro et al. (2004) and from Ferraro et al. (2006), respectively. Models for 47 Tucanae and ω Centauri are from M06.

5.2 Comparison with globular clusters

What are the main differences between BSSs in dSphs and BSSs in globular clusters? Are there any globular clusters whose BSSs behave like those in dSphs? Fig. 8 shows the distribution of $N_{\rm BSS}/N_{\rm HB}$ of Draco and Ursa Minor together with that of 47 Tucanae and ω Centauri (from M06). We chose 47 Tucanae and ω Centauri because they have very different BSS populations.

47 Tucanae is a sort of prototype for BSSs in globular clusters: it clearly shows the bimodal BSS relative frequency, which has been observed in more and more globular clusters in the last few years (Ferraro et al. 1993, 1997; Zaggia et al. 1997; Ferraro et al. 2004; Sabbi et al. 2004; Warren, Sandquist & Bolte 2006; Lanzoni et al. 2007a). The clusters which do not have a bimodal distribution, in general, show only the central peak of BSSs, which rapidly drops outside the core (see e.g. NGC 1904; Lanzoni et al. 2007b).

The bimodal distribution might be explained by requiring that the central peak is populated mainly by COL-BSSs, the external increase is due to MT-BSSs which have not yet sank to the centre, and the minimum of the BSS distribution is connected with the efficiency of dynamical friction (M04; M06). In fact, the position of the minimum has been found to be equal to the maximum distance ($r_{\rm av}$) from the centre at which dynamical friction is able to bring binaries (progenitors of MT-BSSs) into the core within the lifetime of the cluster (M04, M06). In this scenario, globular clusters without the external rise (e.g. NGC 1904) are expected to be poor in mass-transferring binaries, or not to have formed MT-BSSs in the last Gyr.

From Fig. 8, it is clear that the distribution of BSSs in Draco and Ursa Minor is completely different from that of a typical globular

cluster like 47 Tucanae. In particular, it seems that Draco and Ursa Minor have only the peripheral rise of BSSs, and completely lack the central peak. As we already discussed in Section 3, this supports the idea that the central peak in globular clusters is due to COL-BSSs, whereas the external rise is due to MT-BSSs.

Instead, ω Centauri is unique among the globular clusters where BSSs have been already observed. In fact, $N_{\rm BSS}/N_{\rm HB}$ and $N_{\rm BSS}/N_{\rm RGB}$ in ω Centauri are both consistent with a flat distribution. M06 suggested that this distribution might be the product of both the lack of COL-BSSs in the core of ω Centauri (its core density being quite low) and the inefficiency of dynamical friction. In fact, due to the joint effect of a low central density ($\sim 6 \times 10^3$ stars pc^{-3}) and of a high velocity dispersion ($\sim$17 km s^{-1}), the dynamical friction time-scale in ω Centauri is a factor of $\sim$200 longer than in 47 Tucanae. As dynamical friction is inefficient, binaries do not sink into the centre, and the minimum in the BSS distribution does not appear.

In this sense, ω Centauri appears as something midway between the other globular clusters and the dSphs. Different from dSphs, it can still form COL-BSSs in the centre, because its core density is considerably higher than that of dSphs; but its dynamical friction is inefficient in moulding the shape of BSS distribution, exactly as in dSphs. Fig. 8 even suggests the idea of continuity between 47 Tucanae, ω Centauri and the two dSphs: as the central density of the system decreases, the central peak disappears and the BSS distribution becomes less and less concentrated.

In line with this idea is the distribution of $r_{\rm av}$ (see Fig. 8), which in 47 Tucanae and in many other globular clusters is $\sim 10\, r_{\rm c}$, in ω Centauri is $\sim 1\, r_{\rm c}$, while in Draco and Ursa Minor it does not even appear in the plot, because it is consistent with 0 ($r_{\rm av} \lesssim 5 \times 10^{-2}\, r_{\rm c}$).

We note that, apart from the BSS distribution, ω Centauri displays several features which are indicative of an object midway between globular clusters and dSphs: the metallicity spread, the evidences for rotation, the large mass and the low concentration are quite atypical for a globular cluster; so that some authors (Zinnecker et al. 1988; Freeman 1993; Ideta & Makino 2004) claim that ω Centauri is not a real globular cluster, but the nuclear remnant of a dwarf galaxy.

Finally, in Fig. 8 it is also apparent that the level of $N_{\rm BSS}/N_{\rm HB}$ ($\sim$0.05$-$0.4) in Draco and Ursa Minor is comparable with the level in 47 Tucanae and ω Centauri, analogous to most of the globular clusters (see e.g. M06). Thus, we can conclude that the fraction of BSSs versus HB stars in these two dSphs and in globular clusters is similar. This fact indirectly supports the hypothesis that BSS candidates in Ursa Minor and Draco are real MT-BSSs. In fact, if all the BSSs are MT-BSSs, $N_{\rm BSS}/N_{\rm HB}$ should reflect both the ratio of lifetimes and the fraction of stars in suitable binaries, and should be constant for the same turn-off mass and metallicity populations, if the binary fraction is constant.

6 SUMMARY

In this paper, we addressed the problem of BSS candidates in dSphs in general, and in Draco and Ursa Minor in particular. There are two fundamental open questions about BSSs in dSphs: (i) whether they are authentic BSSs or young stars and (ii) what is their formation mechanism?

We analysed both the radial and the luminosity distributions of these stars, and we compared the data with dynamical simulations of BSSs. The main feature of the observed radial distribution of BSSs, normalized to RGB or HB stars, is the absence of a central peak. Even if the young stars' interpretation cannot be dismissed (at least for Draco; see Appendix B), this suggests that BSS candidates in Draco and Ursa Minor are actually true BSSs. Furthermore, the almost flat radial distribution is consistent with theoretical models (M06) for MT-BSSs, i.e. BSSs which formed by mass transfer in isolated binaries. Also, the luminosity distribution, which does not show any correlation with the position of BSSs, agrees with theoretical models of mass-transfer BSS formation.

These findings support the model by M04 and M06, which explains the formation of BSSs by the joint contribution of stellar collisions and mass transfer in isolated binaries. This model was originally developed only for globular clusters, but we find that it works also for dSphs. As predicted by M06, the presence of a central peak in the relative frequency of BSSs is due to COL-BSSs, and can be explained only if both stellar collisions and dynamical friction are efficient. The peak tends to disappear if the central density of the system is too low and/or its dynamical friction time is too long. This idea was confirmed by the absence of any central peak in ω Centauri, and now we find that this result is even stronger in Draco and Ursa Minor.

Low-density systems, where stellar collisions do not occur, can form only MT-BSSs, whose initial distribution mirrors the distribution of the progenitor binaries. The less efficient the dynamical friction, the more the BSS distribution is similar to the distribution of progenitor binaries. This idea is fully supported by Draco and Ursa Minor BSSs: the best-fitting simulations are based on an isothermal distribution between (approximately) the core and the tidal radius, as we would expect for a distribution of primordial binaries.

Furthermore, Momany et al. (2007) recently analysed the BSS candidates of eight dSphs (Draco and Ursa Minor among them) and found a statistically significant anticorrelation between the relative frequency of BSS candidates ($N_{\rm BSS}/N_{\rm HB}$, calculated over the entire galaxy) and the total luminosity of the dSph. If BSS candidates were young MS stars rather than real BSSs, such anticorrelation would not make sense.

Thus, from our analysis as well as from Momany et al. (2007), we conclude that BSS candidates in Draco and Ursa Minor behave like real MT-BSSs, rather than young MS stars. This suggests (even if it does not definitely prove) that Draco and Ursa Minor are 'fossil' galaxies, where star formation was completely suppressed many Gyr ago. This scenario is also confirmed by recent simulations (Mayer et al. 2007), which indicate that Draco and Ursa Minor, two of the closest dSphs to the Milky Way, had all their gas removed $\sim$10 Gyr ago, probably by tidal shocks and ram pressure exerted by the Milky Way. The 'fossil' nature of Draco and Ursa Minor would make them a natural place to study the conditions at the earliest epochs of galaxy formation.

On the other hand, it would be interesting to thoroughly study the nature of BSS candidates in other dSphs, like Sextans, where star formation probably lasted longer. The main goal would be to understand whether, and what fraction of, these stars are authentic BSSs, in order to disentangle the history of BSS formation from that of MS stars.

ACKNOWLEDGMENTS

We thank the referee, T. Maccarone, for the critical reading of the manuscript. We also thank F. D'Antona, F. Ferraro, S. Zaggia and Y. Momany for useful discussions. MM acknowledges support from the Swiss National Science Foundation, project number 200020-109581/1 (Computational Cosmology & Astrophysics). ER acknowledges support from the Netherlands Organization for Scientific Research (NWO) under project number 436016. MM and ER thank the Kapteyn Astronomical Institute of the University of

Groningen and the Institute for Theoretical Physics of the University of Zürich for the hospitality during the preparation of this paper.

REFERENCES

Aparicio A., Carrera R., Martínez-Delgado D., 2001, AJ, 122, 2524 (A01)
Bailyn C. D., Pinsonneault M. H., 1995, ApJ, 439, 705
Battaglia G. et al., 2006, A&A, 459, 42
Bellazzini M., Ferraro F. R., Origlia L., Pancino E., Monaco L., Oliva E., 2002, AJ, 124, 3222
Beers T. C., Almeida T., Rossi S., Wilhelm R., Marsteller B., 2007, ApJS, 168, 277
Benz W., Hills J. G., 1987, ApJ, 323, 614
Benz W., Hills J. G., 1992, ApJ, 389, 546
Bonanos A. Z., Stanek K. Z., Szentgyorgyi A. H., Sasselov D. D., Bakos G., 2004, AJ, 127, 861
Carney B. W., Latham D. W., Laird J. B., Grant C. E., Morse J. A., 2001, AJ, 122, 3419
Carney B. W., Latham D. W., Laird J. B., 2005, AJ, 129, 466
Carrera R., Aparicio A., Martínez-Delgado D., Alonso-García J., 2002, AJ, 123, 3199 (C02)
Chabrier G., 2003, PASP, 115, 763
Davies M. B., Benz W., Hills J. G., 1994, ApJ, 424, 870
Davies M. B., Piotto G., De Angeli F., 2004, MNRAS, 349, 129
Ferraro F. R., Fusi Pecci F., Cacciari C., Corsi C., Buonanno R., Fahlman G. G., Richer H. B., 1993, AJ, 106, 2324
Ferraro F. R., Paltrinieri B., Fusi Pecci F., Cacciari C., Dorman B., rood R. T., 1997, ApJ, 484, L145
Ferraro F. R., Sills A., Rood R. T., Paltrinieri B., Buonanno R., 2003, ApJ, 588, 464
Ferraro F. R., Beccari G., Rood R. T., Bellazzini M., Sills A., Sabbi E., 2004, ApJ, 603, 127
Ferraro F. R., Sollima A., Rood R. T., Origlia L., Pancino E., Bellazzini M., 2006, ApJ, 638, 433
Freeman K. C., 1993, in Smith G. H., Brodie J. P., eds, ASP Conf. Ser. Vol. 48, The Globular Clusters-Galaxy Connection. Astron. Soc. Pac., San Francisco, p. 608
Freitag M., Benz W., 2005, MNRAS, 358, 1133
Fusi Pecci F., Ferraro F. R., Corsi C. E., Cacciari C., Buonanno R., 1992, AJ, 104, 1831
Girardi L., Bertelli G., Bressan A., Chiosi C., Groenewegen M. A. T., Marigo P., Salasnich B., Weiss A., 2002, A&A, 391, 195
Harbeck D., Grebel E. K., Holtzman J., Geisler D., Sarajedini A., 2002, in Grebel E. K., Brandner W., eds, ASP Conf. Proc. Vol. 285, Modes of Star Formation and the Origin of Field Populations. Astron. Soc. Pac., San Francisco, p. 230
Hernandez X., Gilmore G., Valls-Gabaud D., 2000, MNRAS, 317, 831
Hurley J. R., Tout C. A., Aarseth S. J., Pols O. R., 2001, MNRAS, 323, 630
Hurley J. R., Pols O. R., Aarseth S. J., Tout C. A., 2005, MNRAS, 363, 293
Hurley-Keller D., Mateo M., Grebel E. K., 1999, ApJ, 523, L25
Ideta M., Makino J., 2004, ApJ, 616, L107
Irwin M. J., 1985, MNRAS, 214, 575
Irwin M., 1996, in Espinosa J., ed., 7th Canary Islands Winter School
Irwin M. J., 1996, in Rodríguez Espinosa J. M., Herrero A., Sánchez F. eds, Instrumentation for Large Telescopes. Cambridge Univ. Press, Cambridge, p. 35
Irwin M., Hatzidimitriou D., 1995, MNRAS, 277, 1354 (IH95)
Irwin M. J., Lewis J., 2001, New Astron. Rev., 45, 105
Kleyna J. T., Wilkinson M. I., Gilmore G., Evans N. W., 2003, ApJ, 588, L21
Kleyna J. T., Wilkinson M. I., Evans N. W., Gilmore G., 2004, MNRAS, 354, L66
Landolt A. U., 1992, AJ, 104, 340
Lanzoni B., D'Alessandro E., Ferraro F. R., Mancini C., Beccari G., Rood R. T., Mapelli M., Sigurdsson S., 2007a, ApJ, 663, 267
Lanzoni B. et al., 2007b, ApJ, 663, 1040
Lee M. G. et al., 2003, AJ, 126, 2840 (L03)
Leonard P. J. T., 1989, AJ, 98, 217
Lombardi J. C. Jr,Warren J. S., Rasio F. A., Sills A., Warren A. R., 2002, ApJ, 568, 939
Mapelli M., Sigurdsson S., Colpi M., Ferraro F. R., Possenti A., Rood R. T., Sills A., Beccari G., 2004, ApJ, 605, L29 (M04)
Mapelli M., Sigurdsson S., Ferraro F. R., Colpi M., Possenti A., Lanzoni B., 2006, MNRAS, 373, 361 (M06)
Mateo M. L., 1998, ARA&A, 36, 435
Mateo M., Nemec J., Irwin M., McMahon R., 1991, AJ, 101, 892
Mateo M., Fischer P., Krzeminski W., 1995, AJ, 110, 2166
Mayer L., Kazantzidis S., Mastropietro C., Wadsley J., 2007, Nat, 445, 738
McCrea W. H., 1964, MNRAS, 128, 147
McMahon R. G., Walton N. A., Irwin M. J., Lewis J. R., Bunclark P. S., Jones D. H., 2001, New Astron. Rev., 45, 97
Momany Y., Held E. V., Saviane I., Zaggia S., Rizzi L., Gullieuszik M., 2007, A&A, 468, 973
Monkiewicz J. et al., 1999, PASP, 111, 1392
Monkman E., Sills A., Howell J., Guhathakurta P., de Angeli F., Beccari G., 2006, ApJ, 650, 195
Naylor T., 1998, MNRAS, 296, 339
Piatek S., Pryor C., Armandroff T. E., Olszewski E. W., 2001, AJ, 121, 841
Pols O. R., Marinus M., 1994, A&A, 288, 475
Sabbi E., Ferraro F. R., Sills A., Rood R. T., 2004, ApJ, 617, 1296
Sandage A. R., 1953, AJ, 58, 61
Ségall M., Ibata R. A., Irwin M. J., Martin N. F., Chapman S., 2007, MNRAS, 375, 831
Sigurdsson S., Davies M. B., Bolte M., 1994, ApJ, 431, L115
Sigurdsson S., Phinney E. S., 1995, ApJS, 99, 609
Sills A., Bailyn C. D., 1999, ApJ, 513, 428
Sills A., Bailyn C. D., Edmonds P. D., Gilliland R. L., 2000, ApJ, 535, 298
Sills A., Faber J. A., Lombardi J. C. Jr, Rasio F. A., Warren A. R., 2001, ApJ, 548, 323
Tian B., Deng L., Han Z., Zhang X. B., 2006, A&A, 455, 247
Tolstoy E. et al., 2004, ApJ, 617, L119
Walker M. G., Mateo M., Olszewski E. W., Pal J. K., Sen B., Woodroofe M., 2006, ApJ, 642, L41
Warren S. R., Sandquist E. L., Bolte M., 2006, ApJ, 648, 1026
Wilkinson M. I., Kleyna J. T., Evans N. W., Gilmore G. F., Irwin M. J., Grebel E. K., 2004, ApJ, 611, L21
Zaggia S. R., Piotto G., Capaccioli M., 1997, A&A, 327, 1004
Zinnecker H., Keable C. J., Dunlop J. S., Cannon R. D., Griffiths W. K., 1988, in Grindlay J. E., Davis Philip A. G., eds, Proc. IAU Symp. 126, The Harlow Shapley Symposium on Globular Cluster Systems in Galaxies. Kluwer, Dordrecht, p. 603

APPENDIX A: FOREGROUND SUBTRACTION

The contamination of the data due to foreground Milky Way stars (and also to background objects) is quite evident, especially for the RGB region (see Figs 2 and A1). Removing such contamination is important, especially in the outer regions of the dSphs.

We note that, although we refer only to 'foreground' removal, the methods outlined below work equally well for the subtraction of the contamination by compact background objects.

A1 RGB and BSS foreground contamination

In order to estimate the foreground contamination for RGB stars and BSSs, we adopt the following method, both in Draco and in Ursa Minor.

First of all, we assume that all stars redder than $(V - I) = 1.5$ and with V in the [19.5, 23] range (hereafter VRS, i.e. very red stars) are in the foreground. In fact, the VRS region of the CMD (box 5 in

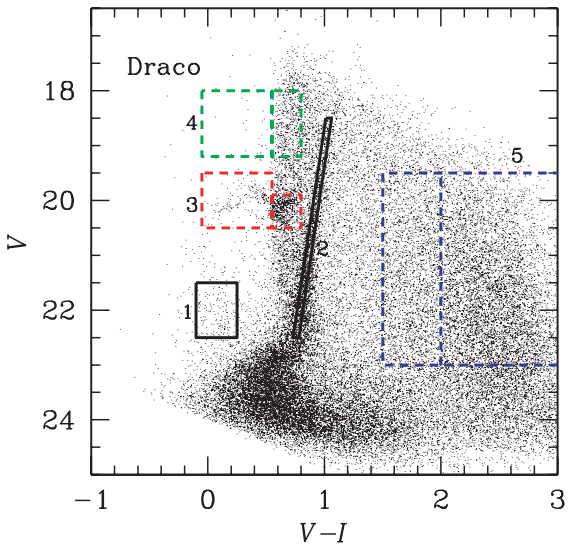

Figure A1. CMD diagram of Draco. As in Fig. 2, the selection areas for BSS (1), RGB (2) and HB (3) are shown. We also show the selection boxes for the HB foreground (4) and the VRS (5).

Fig. A1) should not be populated by stars belonging to Draco, nor to Ursa Minor.[8]

Second, we expect that all the stars which are outside r_t do not belong to the dSph, independent of their colour and magnitude. This is useful because the Draco data extend well beyond r_t, and we can select a subset of 'external' stars, which we define to include all the stars whose elliptical radial distance from the centre exceeds $r_t = 45.1$ arcmin.

We can therefore count the number of VRS, RGB and BSS equivalents[9] with $r_{ell} > r_t$($N_{VRS,\,ext}$, $N_{RGB,\,ext}$ and $N_{BSS,\,ext}$, respectively), and we derive the ratios $f_{RGB/VRS} = N_{RGB,\,ext}/N_{VRS,ext} \simeq 0.0318 \pm 0.0025$, and $f_{BSS/VRS} = N_{BSS,\,ext}/N_{VRS,\,ext} \simeq 0.0031 \pm 0.0008$.

These ratios should be independent of position, as we have tested this in two ways. First of all, we looked for fluctuations of the surface density of VRS stars as a function of radius. Although small fluctuations are present, the overall density can be considered constant in the whole Draco field (it is consistent with a constant value of 0.94 VRS arcmin^{-2}, with reduced $\chi^2 \simeq 0.8$ over 23 radial bins). As a further test, we split the 'external' region into its eastern and western half and checked that there is no statistically significant difference between the values of $f_{RGB/VRS}$ and of $f_{BSS/VRS}$ which were obtained in the two halves.

The foreground contamination of the ith elliptical annulus can be estimated by counting the number $N_{VRS,i}$ of VRS stars in the annulus, and converting it into the expected number of foreground BSSs (RGB stars) through the factor $f_{BSS/VRS}$ ($f_{RGB/VRS}$). Then, the corrected number of BSSs (RGB stars) is simply

$$N_{BSS,i} = N_{BSS,obs,i} - \quad N_{VRS,i}\, f_{BSS/VRS} \tag{A1}$$

$$N_{RGB,i} = N_{RGB,obs,i} - \quad N_{VRS,i}\, f_{RGB/VRS}, \tag{A2}$$

[8] We also checked a more restrictive definition of VRS, i.e. $(V-I) \geqslant 2.0$ and the same V magnitude range. No significant difference was found in our results.

[9] Here, we use the name of BSSs and RGB just for convenience. These are foreground stars which happen to have the same colour and magnitude of BSSs and RGB, respectively.

where $N_{BSS,obs,i}$($N_{RGB,obs,i}$) is the number of BSSs (RGB stars) observed in the annulus.

In the case of Ursa Minor, we do not have enough data at large radial distances from the centre, and therefore cannot obtain a local estimate for $f_{RGB/VRS}$ and $f_{BSS/VRS}$. For this reason, we use the values obtained for Draco also for Ursa Minor. This is not optimal, but also not unreasonable, as the two dSphs are at comparable Galactic latitudes.

A2 HB foreground contamination

The above procedure for RGB and BSSs could also be used for HB stars. However, for HB stars we adopt a more straightforward technique, making use of the fact that the foreground does depend on colour, whereas it is nearly independent of magnitude (at least in the range considered in our CMD).

Such a fact cannot be exploited in the case of RGB and BSSs, because it requires a CMD region which is both in the same colour range as BSSs or RGB and populated by foreground stars only. However, for HB stars, the dashed regions labelled as 4 in Fig. A1 are at exactly the same $(V-I)$ range of the regions (labelled 3) where HB stars are selected, and are almost exclusively populated by foreground stars.

In order to account for the different foreground level for RHB and BHB stars, we further divided Region 4 of Fig. A1 into two subregions: a blue one with the same colour range of BHB and a red one with the same colours of RHB. We will refer to stars in the two subregions as to the fgBHB, and the fgRHB stars, respectively.

Then, the corrected numbers of RHB (BHB) stars in the ith annulus are

$$N_{RHB,i} = N_{RHB,oss,i} - N_{fgRHB,i}\,\frac{A_{RHB}}{A_{fgRHB}} \tag{A3}$$

$$N_{BHB,i} = N_{BHB,oss,i} - N_{fgBHB,i}\,\frac{A_{BHB}}{A_{fgBHB}}, \tag{A4}$$

where $N_{RHB,oss,i}$($N_{BHB,oss,i}$) is the number of RHB (BHB) stars which was actually observed in the annulus, $N_{fgRHB,i}$($N_{fgBHB,i}$) is the number of fgRHB (fgBHB) stars in the annulus and A_{RHB}/A_{fgRHB}(A_{BHB}/A_{fgBHB}) is a correction factor which accounts for the different extensions of the various regions in the CMD.

Foreground subtraction is then carried out by subtracting the number of fgBHB (fgRHB) stars in the annulus (after a correction accounting for the ratios of the CMD areas) from the number of BHB (RHB) stars in the annulus.

We note that this method of foreground subtraction has a slight dependence on the radial distance, the foreground level within the core radius being generally higher than outside. This is because, in addition to subtracting Milky Way stars in the foreground component, this technique also accounts for extra-effects (like binaries, blending, errors in the observed magnitude and contamination from other stellar types, like RGB).

As a sanity check, we compared the distribution of HB stars obtained by using this method of foreground subtraction and that obtained using the same procedure as for RGB and BSSs. The differences in the inner annuli are negligible. In the outer annuli ($>2\,r_c$, where r_c is the core radius) the difference is larger, but remains within the (quite large) Poissonian error bars.

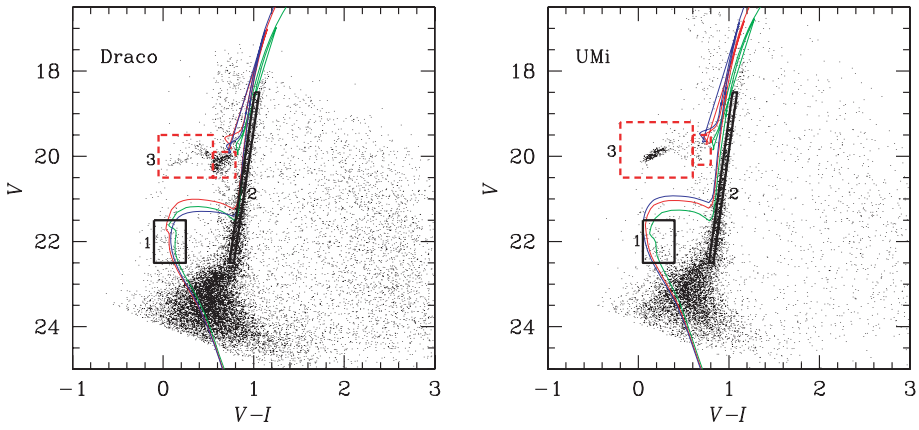

Figure B1. Reddening and distance-corrected isochrones of single stellar populations superimposed to the CMD of the central region of Draco (left-hand panel; here, in order to reduce foreground contamination, we plot only stars with $r \leqslant 28.3$ arcmin) and Ursa Minor (right-hand panel). In both cases, the left line refers to a metallicity [Fe/H] $= -2.3$, the middle one to [Fe/H] $= -2.0$ and the right one to [Fe/H] $= -1.5$. We assumed ages of 2.0 and 2.5 Gyr in the case of Draco and Ursa Minor, respectively. Boxes are the same as in Fig. 2.

APPENDIX B: A TEST OF THE YOUNG STAR HYPOTHESIS THROUGH ISOCHRONES

Although we have shown that the properties of the observed BSS population are fully compatible with the expectations for 'real' BSSs, the 'young star' interpretation provided by A01 for Draco still remains viable.

A more direct test of the nature of this population can be performed by looking for other hints of a relatively young population. Actually, the A01 interpretation of the BSSs in Draco was based on the observation of a small concentration of stars in a region of their CMD (the 'red clump', i.e. Region 13 of their fig. 13) which should not be populated if no star formation occurred in the last 10 Gyr.

We performed a similar test by means of the isochrones of the Padova group (see Girardi et al. 2002; see also http://stev.oapd.inaf.it/∼lgirardi/cmd).

We plotted a set of theoretical isochrones over the Draco and Ursa Minor CMDs,[10] varying both the age and the metallicity of the stellar population (see Fig. B1 for some examples). From such isochrones, it is clear that BSSs lie close to the isochrones describing low-metallicity ([Fe/H] $\leqslant -1.5$, perfectly compatible with current estimates for Draco and Ursa Minor) stellar populations with ages between 2 and 3 Gyr.

For Draco, we chose to combine a Chabrier (2003) lognormal IMF with an isochrone for an age of 2 Gyr and a metallicity [Fe/H] $= -2.0$ in order to estimate the number of stars which should be expected in other regions of the CMD if all of the observed BSSs are actually part of an intermediate-age population. Within this scenario, the regions where we expect the maximum number of intermediate-age stars and the minimum contamination from the old population are as follows:

(i) the young MS just below the BSS selection box;
(ii) the bright and faint part of the BSS selection box;
(iii) the red clump.

Table B1. Comparison of isochrone predictions (age 2.0 Gyr, [Fe/H] $= -2.0$.) with observations for Draco.

CMD region	$N_{\rm pred}$	$N_{\rm raw}$	$N_{\rm fg}$	$N_{\rm obs}$
Young MS	36.8 ± 3.4	43	2.3	40.7 ± 7
BSS faint	84.2 ± 7.7	76	2.3	73.7 ± 9
BSS bright	36.8 ± 3.4	45	3.0	42.0 ± 7
Red clump	15.3 ± 1.4	101	53.3	47.7 ± 11

In Table B1, we list the theoretical predictions from the isochrones ($N_{\rm pred}$), the total number of stars observed in each CMD region ($N_{\rm raw}$), the estimated foreground contamination ($N_{\rm fg}$) and the number of observed stars after the foreground subtraction ($N_{\rm obs}$).

It is clear that the predictions from the young star hypothesis are quite compatible with our observations of Draco: the ratio of faint BSSs to bright BSSs is slightly lower than expected (1.75 ± 0.49 instead of 2.29), but the difference is just at the 1σ level; on the other hand, the predicted number of young MS and red clump stars is perfectly compatible with observations, as both these CMD regions are likely to be contaminated by the old Draco stellar population (old MS stars close to the turn-off for the young MS region, RGB and especially – given the partial superposition of the two regions – HB stars for the red clump region).

We applied the same method also to Ursa Minor, using an isochrone age of 2.5 Gyr. Results are summarized in Table B2,

Table B2. Comparison of isochrone predictions (age 2.5 Gyr, [Fe/H] $= -2.0$.) with observations for Ursa Minor.

CMD region	$N_{\rm pred}$	$N_{\rm raw}$	$N_{\rm fg}$	$N_{\rm obs}$
BSS faint	63.6 ± 6.4	71	1.0	70.0 ± 9
BSS bright	36.3 ± 3.7	29	1.0	28.0 ± 6
Red clump	11.4 ± 1.2	28	16.2	11.8 ± 6

[10] We assumed a reddening $E(B-V) = 0.03$ for both galaxies, a value for which a vast consensus exists. The distance modulus of Ursa Minor was chosen to be 19.41 [Bellazzini et al. (2002), and C02 found 19.41 ± 0.12 and 19.40 ± 0.10, respectively]. The distance modulus of Draco is more controversial, as recent determinations yielded relatively different values: A01, and Bonanos et al. (2004) found compatible values (19.5 ± 0.2 and $19.40 \pm 0.15 \pm 0.02$, respectively); but Bellazzini et al. (2002) found a significantly higher value (19.84 ± 0.14). We adopted the intermediate value of 19.60. We cannot make an estimate from our data, as the tip of the RGB in our WFC data is beyond the saturation limit.

where we omitted the Young MS region because of the very strong contamination from the old MS. The number of stars in the red clump region appears to be extremely close to the prediction from the young stars hypothesis, but a strong contamination is surely present, as the red clump selection box [$19.62 \geqslant V \geqslant 19.12$, $0.90 \geqslant (V - I) \geqslant 0.50$] largely superimposes with the HB (see Fig. B1). Such a strong contamination accounts for most of the 'excess' stars in the considered CMD region. However, the young star hypothesis might still be viable, because most of the red clump stars might be 'hidden' within the HB.

In summary, the interpretation that BSS candidates in Draco are intermediate-age stars can neither be ruled out nor be confirmed by the isochrone method applied to our observations. Only a spectral analysis of stars in the red clump region could solve the uncertainty. In Ursa Minor, such an interpretation is hardly compatible with current data (see also C02), but cannot be completely ruled out.

We point out that in both galaxies the mass of the intermediate-age population needed to explain the BSS candidates is just about $10^4\,M_\odot$, which is a very small fraction of the mass of Draco or Ursa Minor. If the age spread is $\gtrsim$1 Gyr, the implied star formation rate is $\lesssim 10^{-5}\,M_\odot\,yr^{-1}$, comparable to the estimates shown in figs 14 and 16 of A01, and much lower than any observed star formation rate in dwarf galaxies.

Finally, the isochrones can also be used to give an indicative estimate of the upper/lower limit mass of BSSs, which are used to set up our simulations (see Section 4). For Draco, we find that their masses should be in the range $1.11-1.35\,M_\odot$, whereas for Ursa Minor this range moves slightly to $1.09-1.34\,M_\odot$.

This paper has been typeset from a TEX/LATEX file prepared by the author.